One-step deposition by slot-die coating of mixed lead halide perovskite for photovoltaic applications

Giovanni Cotella, Jenny Baker, David Worsley, Francesca DeRossi, Cameron Pleydell-Pearce, Matthew Carnie, Trystan Watson[1]

SPECIFIC, Swansea University, Bay Campus, Fabian Way, Crymlyn Burrows, Swansea, SA1 8EN, Wales UK

Abstract

Recent advances in the performance and stability of lead halide perovskite solar cells announce a promising future for this technology. As the understanding of lab scale device fabrication progresses technology developments in the area of up-scaling are required to demonstrate their viability on an industrial and pre-commercial scale. These developments include replacing slow spin coated deposition techniques with continuous roll to roll compatible slot-die methods. In this work we demonstrate the suitability of a one-step slot-die coating method for the deposition of lead halide perovskite layers, in particular for infiltration into a mesoporous titania scaffold. Appropriate crystallisation dynamics of the perovskite are achieved by careful control of the substrate temperature in combination with a post-processed rapid air knife application. We show that devices fully processed in air using this method deliver a photovoltaic conversion efficiency up to 9.2% , this is comparable to those manufactured using a spin coating process.

Keywords: Perovskite, slot-die, printing, one-step, photovoltaic

1. Introduction

There are a number of photovoltaic technologies such as organic, dye sensitised, perovskite and quantum dot solar cells which aim to capitalise on the lower manufacturing cost achievable through solution processing combined with low embedded energy costs[1–3]. Since 2012, perovskite solar cells have emerged as the most efficient of the solution processed PV technologies [4, 5] with more recent advances demonstrating devices with efficiencies over 20%

[6]. Progress on the lifetime of perovskite based devices, up to 1000 hours under full AM 1.5 simulated sunlight in ambient air [7–9], suggests that perovskite solar cells are a promising technology for the transition to industrial scale manufacture.

In addition to improvements in materials, to increase efficiency and lifetime, methods of deposition must also evolve in order to progress the technology from the laboratory into production. For fundamental studies at laboratory scale, spin coating is often favoured as a convenient method to deposit solution processed solar cells [4, 10, 11]. However, spin coating is limited in commercial production by the high percentage of material wastage, necessity for batch processing and constrained substrate size.

Techniques compatible with roll to roll deposition such as slot-die coating [12, 13] flexographic printing [14] blade coating [15] and K-bar [16] deposition have been used for solar cell production and have the added advantage that there is typically less materials wastage than spin coating because of the direct deposition of material onto the substrate. This direct deposition has a disadvantage that the dynamic drying of the solvent, which is associated with spin coating [17] does not occur and so all solvent removal must be achieved during subsequent heating steps. When crystallising perovskite from a precursor solution of lead chloride and methyl ammonium iodide in a single step process this excess solvent affects the crystallisation dynamics and if not controlled can lead to vertical crystal growth which causes a rough perovskite layer with poor surface coverage and therefore low photocurrent.

Single step deposition of perovskite by scaleable techniques such as spray coating [18] doctor blading [19–22] and slot-die coating [12] have been shown to give good coverage when deposited onto a PEDOT:PSS layer in an inverted p-n type architecture but when deposited onto a metal oxide layer the crystallisation dynamics are unfavourable and poor coverage of the perovskite is achieved, limiting photocurrent [12].

In terms of long-term stability, it has been reported that planar cells with inverted device architecture and water-based PEDOT:PSS as the HTM onto the ITO substrate, can easily degrade [23] due to the hygroscopic and acidic nature of PEDOT, ease of diffusion of PSS into other layers and instability of the ITO/organic interface [24, 25]. Planar cells with conventional architecture have not shown satisfying lifetime so far [26, 27] with only limited studies demonstrating higher long-term stability when using a combined halide perovskite [28], a water-free PEDOT:PSS [29] or a vacuum-assisted thermal annealing process to completely remove organic chloride by-products [30]

It is thus more advantageous to use an architecture based on a metal oxide scaffold, since this has been shown to exhibit improved stability, up to 1000 hours both in the dark [31] and under full illumination [8, 32] compared to planar counterparts (inverted or not) [24].

In order to improve the surface coverage of perovskite deposited onto a mesoporous titania scaffold, a two-step process can be employed [32] where first lead iodide is deposited from solution and this is converted into perovskite by immersion into methyl ammonium iodide [15]. This has enabled the perovskite to be deposited by slot-die coating of PbI_2 supported by air quenching [33] however in order to convert the lead iodide into perovskite a second coating step must be employed which adds to the complexity of the processing. Of the roll to roll compatible processes, slot-die coating is favoured since it can produce patterned layers eliminating the need for complex removal steps associated with un-patterned deposition [15]. By using an airknife to control the temperature gradient, combined with a preheated substrate, the crystallisation dynamics can be controlled and this work demonstrates for the first time a single step deposition by slot-die coating of perovskite onto a mesoporous titania scaffold.

2. Materials and Methods

2.1. slot-die coating trials (temperature and air-knife setup)

Plain soda glass (100mm x 150mm) substrates were cleaned with Hellmanex and then sequentially rinsed with de-ionized water, acetone, isopropanol, ethanol before being oxygen plasma treated. A 40 wt% solution of methylammonium iodide (MAI) and $PbCl_2$ (3:1 molar ratio) in DMF was prepared in a nitrogen atmosphere. The solution was then transferred to a class 10,000 clean room maintained at an average relative humidity below 50%. The solution was pumped into the slot-die coating head, kept at 40°C to avoid issues due to PbI_2 crystallisation. To test the influence of substrate temperature on coating condition this was varied between 20°C (no external heating source), and 65°C or 90°C achieved by preheating the substrate for 30 minutes in an oven prior to application of the material. The distance between meniscus waveguide and glass substrate was set at 50 µm, the pumping rate at 91 µL/min and the coater belt speed at 4.2 mm/sec. When necessary, a cold air knife impinging on the coated layer, with air pressure of 0.5 bar, was placed at a distance of 200 mm horizontally from the coating head and at a height of 250 mm from the sample. Coated precursors were annealed

via two runs in a 2.6m long convection belt oven (Thieme) at 110°C at a belt speed of 3.3 mm/sec. Layer features have been investigated through optical microscopy and stylus profilometry measurements. The print head in operation and the subsequent layers produced are shown in figure 1.

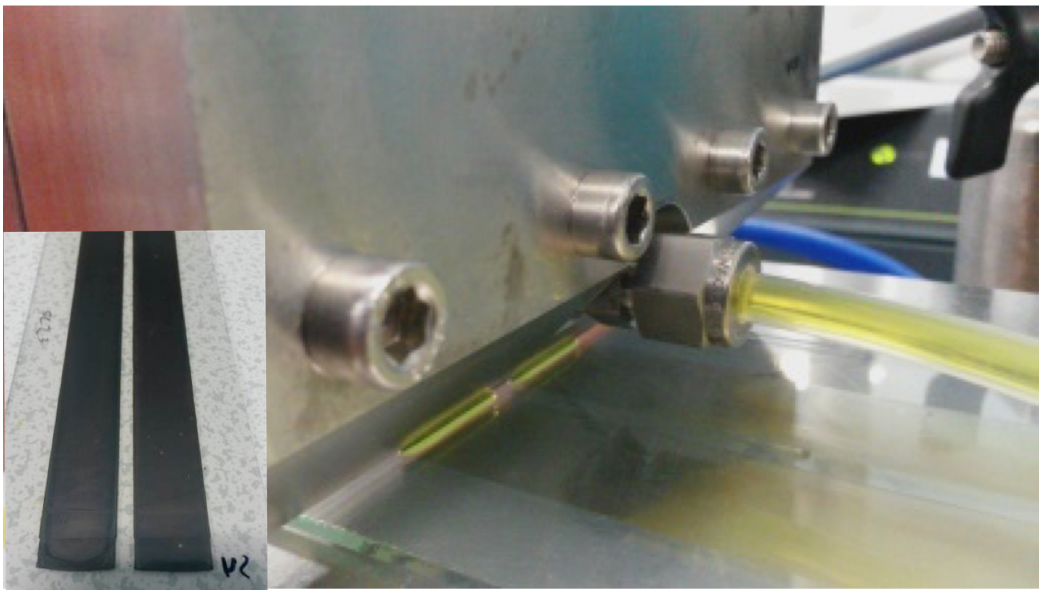

Figure 1: Photograph of the print head in operation. Inset, perovskite layers post deposition and annealing.

2.2. Device Fabrication

Patterened FTO glass substrates were cleaned and plasma treated as described in section 2.1. A compact titania layer (50 nm) was deposited via spray pyrolysis at 300°C from a solution of 1:10 titanium diisopropoxide bis(acetylacetonate) and isopropanol, substrates underwent a sintering step at 550°C for 30 min. For spin coated devices a TiO_2 paste (DSL18NRT) diluted in ethanol (2:7 in weight) was spun over the samples at 5000 rpm, heated at 150°C for 15 minutes and sintered at 550°C for 60 minutes in order to give a 300nm mesoporous layer. Perovskite precursor solution (see section 2.1) was deposited at 2000 rpm, then the substrates were heated for 90 minutes at 100°C. For slot-die coated devices a TiO_2 paste diluted in ethanol (1:1 in weight) was bar coated over the 100mm x 150mm substrate, then it was heated at 150°C for 15 minutes and sintered at 550°C for 60

minutes. Bar coating was used to deposit the mesoporous TiO_2 layer as limitations related to spin coating sample size did not allow large enough substrates to enable a slot-die coating run, see figure 1. This different approach led to an increased mesoporous TiO_2 layer, approximately 350nm for spin coating and 600nm for bar-coating. The precursor solution was pumped into the slot-die coating head and subsequently deposited over the bar-coated mesoporous layer held at a predetermined temperature (20°C, 65°C and 90°C) and subjected to a single pass under the cold air knife. The sample was then transferred to the belt oven, set at 110°C, for two passes according to the parameters noted in section 2.1. The temperature profile of the belt oven can be seen in figure S1 (supplementary). In order to compare performances between cells differentiated only by the mesoporous titania thickness and perovskite layer processing method, slot-die coated samples were scored and reduced in active area to ensure the same device configuration and post processing of subsequent layers (HTM and Au). For the hole transport layer, a 10 wt% solution containing 2,2,7,7-tetrakis-(N,N-di-p-methoxyphenyl-amine)-9,9-spirobiuorene (Spiro-OMeTAD), doped with 4-tert-Butylpyridine and lithium bis-trifluoromethanesulfonimide and oxidised through the addition of vanadium oxide (V_2O_5) [11], was spin coated over the perovskite layer in a nitrogen atmosphere at 2000 rpm. In case of spin coated devices, an additional step was necessary to scrape off the perovskite in order to allow the deposition of the front contact. This step was not necessary in case of slot-die coated devices because this technique produces patterned coatings. Gold contacts were thermally evaporated to complete the device stack.

2.3. Film characterisation

The device nano-structure was characterised using a Carl Zeiss Crossbeam 540 FIBSEM completed with Oxford 50 mm^2 SDD EDS detector, via the preparation of electron transparent lamellar of approximately 100nm in thickness. X-ray diffraction spectra of spin and slot-die coated cell stack (just before the Spiro-OMeTAD deposition) were collected on a D8 Discover (Bruker) x-ray diffractometer with a Cu $K\alpha$ source ($\lambda = 1.5418$ $\mathring{A}$). The step time was 0.2 s and the step increment was 0.01°.

2.4. Device Characterization

I-V testing was carried out using an Oriel solar simulator with a KG5 filter and a Keithley 2400 source meter. The cells were measured at a scan

rate of 0.15 V/s between -0.1V and 1.1V. Ten seconds of light soaking time was applied before each measurement. For all devices an active area of solar cells was defined through a metal aperture mask with an area of 0.0625cm^2. Stabilised current density measurements were carried out whilst maintaining the cells at a voltage corresponding to the maximum generated power for 50 seconds. External quantum efficiency measurements were collected using an QE X10 spectral response machine in the wavelength range between 300 nm and 850 nm. For lifetime measurements, the best performing devices were stored in a humidity controlled environment (30% RH), in the dark and tested at 0, 168, 504 and 1076 hours after their fabrication.

Transient photovoltage decays were measured as described previously [34]. The white bias light was provided by a BRIDGELUX 9000 lumen LED array (Farnell) whilst the pulse light was provided by a OSLON PowerCluster green LED array (RS). Pulse intensity was chosen to ensure ΔV remained within the small perturbation regime. A pulse length of 10 µs was utilised and was generated via a fast MOSFET transistor controlled by a National Instruments USB-6251 data acquisition board (DAQ) and WaveMetrics IGOR Pro software. Currents were measured by the DAQ as a voltage drop across a 30 Ω resistor. The open circuit voltage was allowed to equilibrate for $>$ 60 s before the perturbation pulse was fired. The variance in photovoltage in the preceding 10 s before the perturbation pulse was fired was found to be, on average, $<$ 1.2 mV. A biphasic photovoltage decay was observed and fit with a double exponential function. The faster of the two resultant time constants was taken as the effective recombination lifetime.

3. Results and Discussion

3.1. Influence of substrate Temperature and air knife post processing

Initial studies which entailed depositing the perovskite directly onto the plain glass substrate at room temperature led to an uneven surface structure which exhibited high roughness (average 1.45 µm) and pinhole distribution (Figure 2a), both well known to prohibit good device performance through poor interfacial contact with the hole transporter and increased shunt losses. It was determined that the issue of roughness is likely caused by differential crystallisation rates, strongly influenced by the temperature gradient generated between the top and bottom region of the liquid layer within the first minute after the coating. The solution is kept at 40°C in the coating head, however once it contacts the substrate (which is 20 °C) it cools down in order

to reach thermal equilibrium. Typical of perovskite, this temperature reduction does not trigger a heterogeneous nucleation process, the coated liquid film remained clear after the deposition. However the low temperature induces a slow solvent evaporation rate and enormously reduces the diffusion of the solute within the layer, strongly affecting the nuclei growth rate [35]. Thus when subsequently placed in an oven, which has a top-down hot air stream, there are only a few nuclei within the system surrounded by a solution at room temperature. Once the top of the solution is warmed up by the oven, the growth rate, which follows the temperature gradient, becomes higher in this region enhancing the non-ideal growth of the nuclei in the vertical direction, giving a final layer presenting thick and well separated crystal clusters. In order to promote rapid drying dynamics similar to the spinning process and generate a thermal gradient which promotes the crystal growth horizontally instead of vertically, the substrate material was pre-heated to 65°C and 90°C. The higher temperature gave poor surface coverage however the intermediate temperature led to an increased surface coverage from 65% at 20°C to 72% at 65°C (as measured using colour thresholding software, ImageJ). These are shown in figure 2 (a and b).

In addition to improved surface coverage the pre-heated substrates produced thinner layers, 960nm at 65°C. Moreover the average roughness (Ra) reduced from 180nm at 20°C to 134nm at 65°C, this is shown graphically in figure 2 (d). In this case a faster solvent evaporation creates a rapid increment of precursor concentration triggering heterogeneous nucleation with a large number of events over the warm surface. The reduction of the liquid content, which turns the coated layer dark yellow and which we attribute to initial nuclei growth, was a process fairly visible with unaided eyes, just a few seconds after deposition. In this case an opposite thermal gradient is generated within the solution compared to the 20°C substrate. Indeed the higher temperature at the liquid-solid interface makes the crystals grow faster in this region. When crystal growth approaches the colder region of the liquid film, the solute feeding flux caused by thermal convective motions, becomes strongly anisotropic affecting the crystal growth direction and rate. In particular, the horizontal component (parallel to the substrate surface) of the growing vector becomes predominant since the vertical one is drastically reduced because of the negative temperature gradient. This condition forces the crystals to grow along the warm region of the solution resulting in a levelling effect over the sample. A schematic representation of the described layer differences is illustrated in figure 3a.

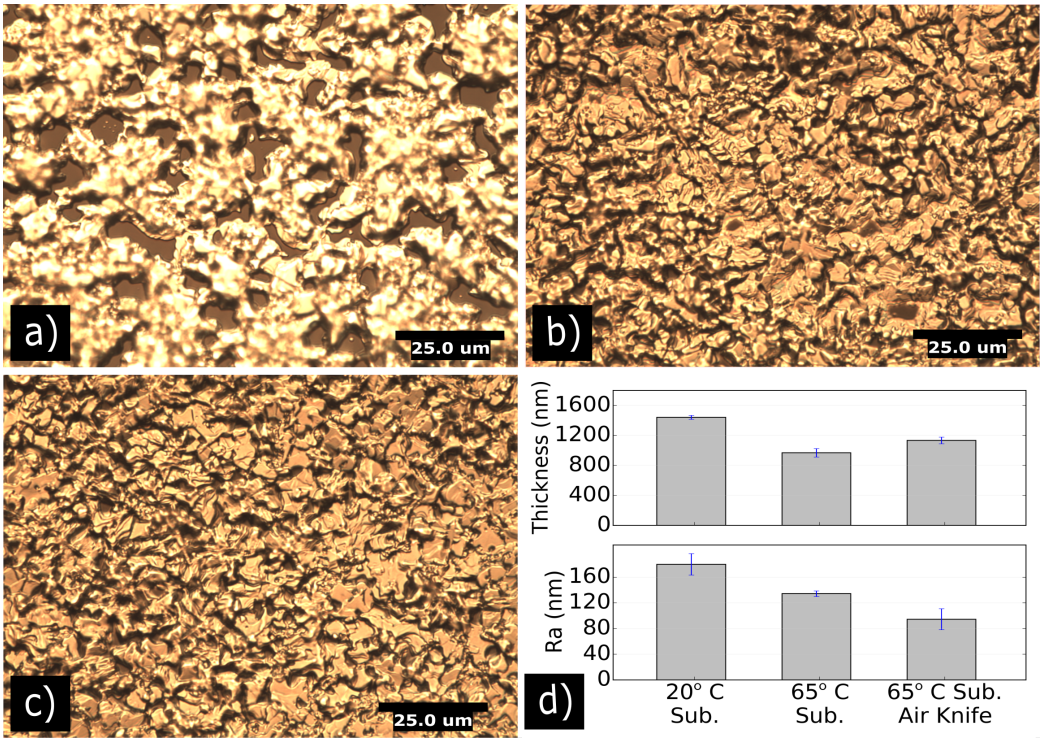

Figure 2: Effect of substrate temperature and air knife on the slot-die coated mixed halide perovskite layer on glass substrate. Optical microscope and profilometric measurements a) Substrate at 20°C), b) Substrate at 65°C, c) Substrate at 65°C with air knife applied. d) Average layer thickness and roughness of samples

Further reduction in perovskite roughness, down to 95nm can be achieved through the use of a cold air knife applied just after the slot-die coating of the perovskite precursor (figure 2 c). Figure 3 b illustrates the same crystallisation process but in the presence of a pressured air knife blowing over the just coated perovskite precursors. In this case, the intense air flow subtracts a larger amount of thermal energy and creates an even stronger temperature gradient between the upper and lower region of the coated solution, allowing better control over the crystallisation process and giving a stronger flattening effect, as demonstrate by the marked reduction of the average roughness of such samples. The cold air-knife was applicable only in case of warm substrates thanks to the rapid reduction of liquid content while in case of cold substrate, the thick liquid layer was simply moved ahead by the air pressure applied.

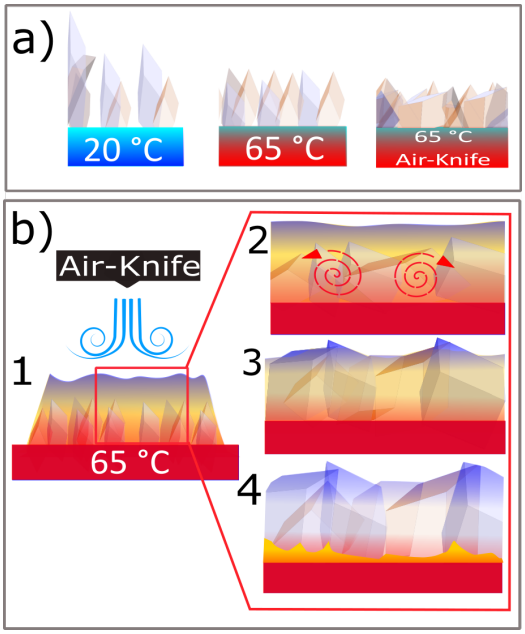

Figure 3: Crystallisation Process. a) Illustration of the layer differences obtained with substrate at 20°C, preheated to 65°C and 65°C with air kinfe b) 1. Application of air knife following initial formation of crystal nuclei. 2. Convective motions and reduced viscosity boost the crystal growth at the interface with the substrate 3. Crystals approach the cooler region reducing the vertical growth rate in favour of lateral growth across the warm substrate. 4. Reduced thickness is achieved.

Glass was used as a substrate to demonstrate the crystallisation process as perovskite precursor solution exhibits complete wetting on a mesoporous TiO_2 film as the solution is absorbed into the mesoporous substrate. The use of a glass substrate for these experiments allows a greater understanding to be developed about the formation of the capping layer on top of the infiltrated mesoporous film. However replicating this study on mesoporous TiO_2 with a perovskite capping layer gave the same trend in roughness and surface coverage as shown in Figure S2.

3.2. Device performance

In order to prove the scalability of the perovskite layer in complete devices the precursor solution was slot-die printed entirely in an ambient environment maintaining the substrate at 65°C and using the cold air-knife in order to reduce the layer thickness and roughness, devices were also prepared without the heated substrate or air blade for comparison. A conventional n-i-p

architecture was adopted using TiO_2 as both a compact blocking layer and as a mesoporous scaffold. For annealing a 2.6m belt oven was adopted in order to replicate potential industrial conditions (the oven temperature profile is shown in figure S1). Comparison spin coated devices were prepared in a nitrogen filled glovebox environment using a hot plate for annealing. PCE data is shown in Figure 4.

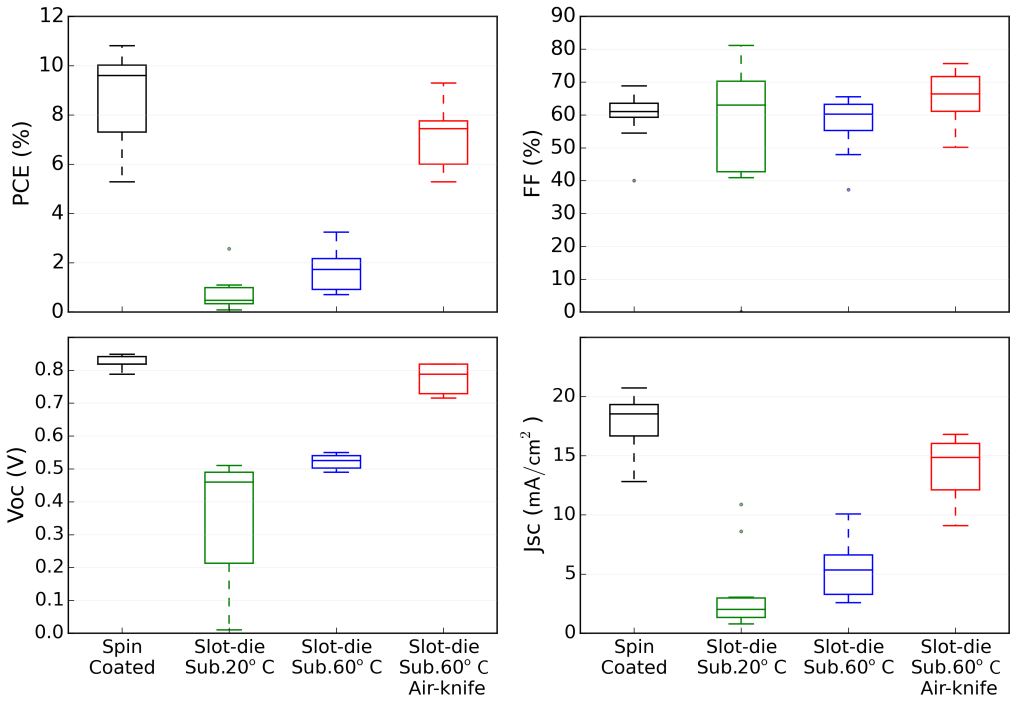

Figure 4: Statistics of spin and slot-die coated perovskite cells performances. From the top left corner: power conversion efficiency (PCE), fill factor (FF), short circuit current density (J_{SC}), open circuit voltage (V_{OC}). The data set comprises 10 devices for each process.

Interestingly we did not observe a dramatic difference in device performances between the spin coated and optimised slot-die method. In particular, slot-die coated perovskite cells showed an average PCE of 7.0 %, with champion device performance resulting in 9.2%. Devices fabricated entirely through spin coating in a nitrogen atmosphere reached performances slightly higher, achieving an average PCE of 8.8%. The highest spin coated device achieved a PCE of 10.8%. The slot die coated samples with no air-knife or

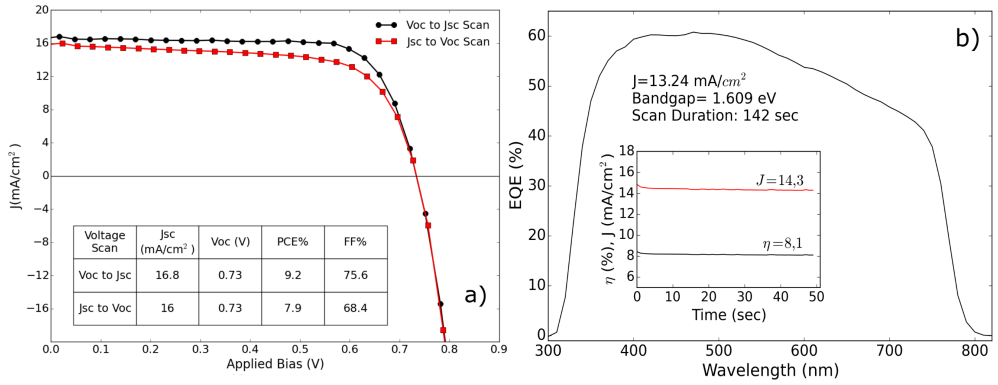

Figure 5: Best slot-die coated cell performances. a) JV curves for reverse (black dots) and forward (red squares) scan. The inset table collects the cell performances for each measure. b) External quantum efficiency measurement. The inset graph represent the stabilised current density and efficiency over the time. As expected the integrated current density matches pretty well the stabilised one.

preheated substrate showed the worst average PCE of 0.7%. The maximum PCE was 2.4% The samples with the substrate at 65°C and no airknife had higher average performance of 1.7%, due mainly to more consistent current and V_{OC} characteristics. The maximum PCE was 3.2%.

Figure 5 shows the forward and reverse JV curves for the best performing slot-die coated devices alongside EQE and stabilised current. Remarkably the cell presents very low hysteresis and a stabilised current value that matches reasonably with the integrated current resulting from the EQE measurement.

Variation in performances between the two methods can be ascribed to the varying amount of perovskite applied between the two deposition techniques. The spin coated perovskite cells have an approximate TiO_2 thickness of 300nm with a perovskite capping layer approximately 75nm whereas the slot die coated perovskite cells have an approximate TiO_2 thickness of 600nm and a perovskite capping layer of approximately 200nm

Figure 6 shows transient photovoltage (TPV) decay data for typical spin and slot-die coated devices. The decays obtained were typically bi-exponential as observed previously [36] and a double exponential function was used to fit to the decays generating two time constants. The decay lifetimes (Tau) shown in figure 6 are the faster of the two time constants, which is reported to represent recombination lifetime in perovskite devices [37]

Looking at Figure 6 it can be seen that recombination is an order of

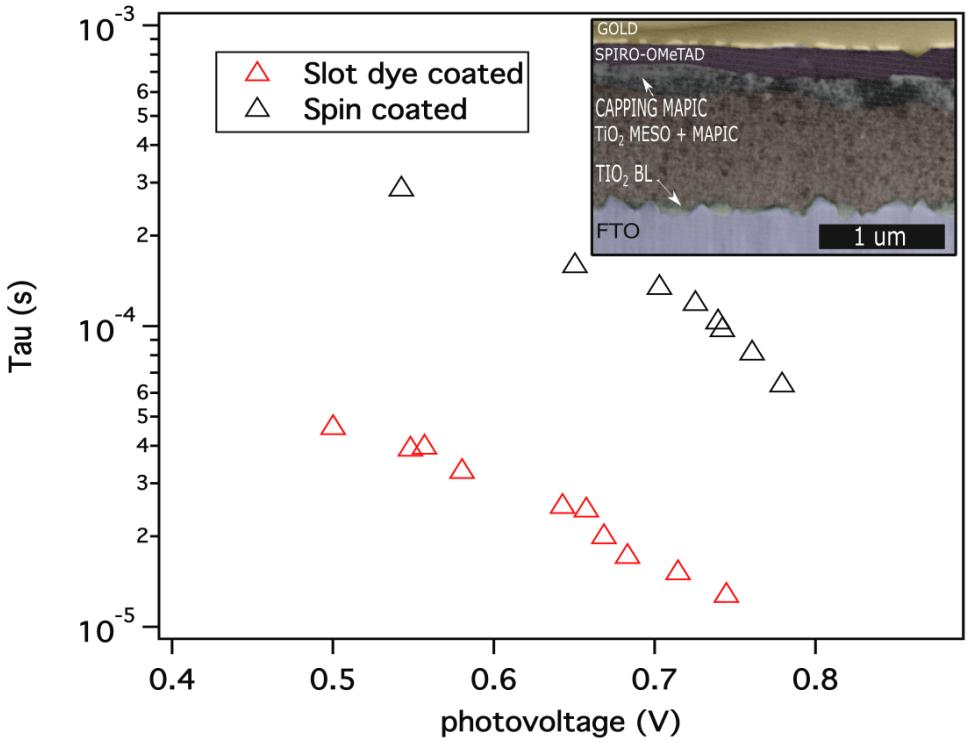

Figure 6: Transient photovoltage decay data of spin-coated and slot-dye coated devices. The decay lifetime is significantly faster in the slot-dye coated devices, indicating faster recombination. Figure 6b inset SEM cross-section of slot-dye coated device showing combined TiO_2 MAPIC layer.

magnitude faster in the slot-die coated device compared to its spin-coated counterpart. Diffusion lengths in MAPIC are reported to be of the order of 1 micron [38] and so as film thickness approaches the diffusion length, it might be expected that the rate of recombination will also increase. The faster recombination in the slot-die device can be attributed to the thicker perovskite layer and may be the cause of lower voltages. A faster rate of recombination might also be expected to reduce fill factors but this is not the case here. The higher fill factors seen in slot-die coated devices may also be an artefact of film thickness in that the thicker perovskite capping layer prevents the spiro-OMeTAD from contacting the m-TiO_2 layer making a shunt contact less likely. The reduction in photocurrents observed in slot-die coated devices may also be linked to increased recombination. X-ray diffraction was performed to investigate crystallographic differences between the two different processing methods. As displayed in Figure 7, XRD results are in good agreement with a tetragonal symmetry [39].

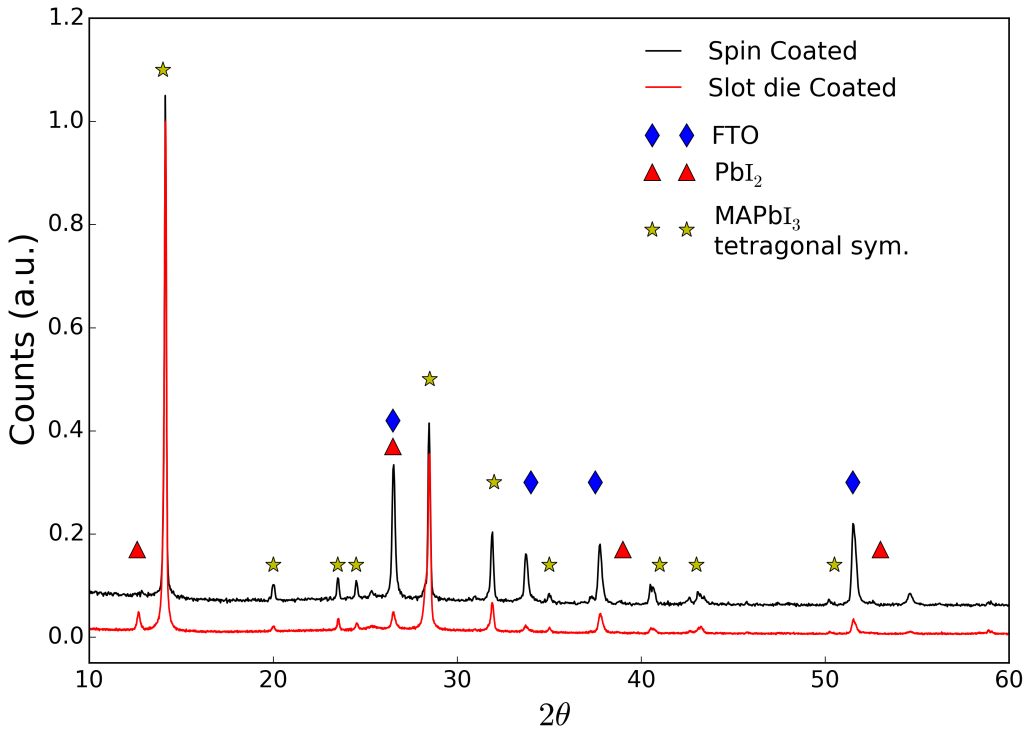

Figure 7: X-Ray diffraction spectra of spin coated and slot-die coated perovskite solar cells.

Peaks associated with the lead iodide are indicated by red triangular markers, it is possible to observe that the predominant peak (at $2\theta = 12$) is present only in the case of the slot-die coated devices. This suggest that the slot-die method has not achieved full conversion of the perovskite precursor solution. Although the peak is small it is likely that this is a contributor to the reduced current observed for this method.

Shelf life testing (dark storage conditions at room temperature) was carried out on the slot-die coated devices. Devices were removed periodically and measured under a solar simulator at 1 sun. Figure 8 shows the main PV characteristics with storage time.

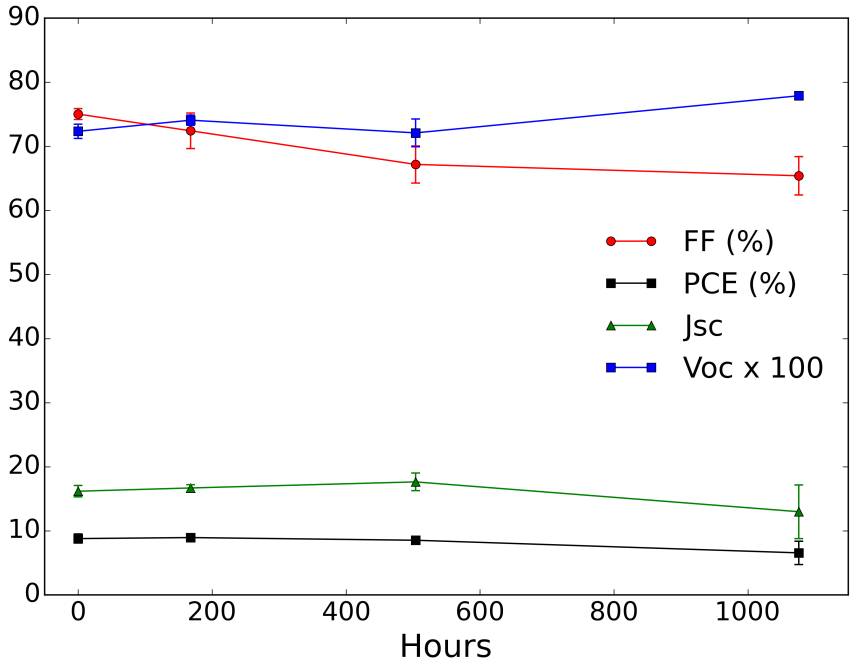

Figure 8: Shelf life test on best performing slot-die coated perovskite devices. Unencapsulated cells were stored in a humidity controlled environment (30%) in the dark and measured at 0, 168, 504, 1076 hours following fabrication. Average values (3 devices) and standard deviations are plotted.

We observed a generally flat overall evolution in device performance over time, with a 7.0 % V_{OC}) increment while J_{SC}) and FF reduced by 19.7% and 12.8% respectively, resulting in an average 25.5% reduction of the PCE

(from 8.8% to 6.5% on average) after over 1000h. These devices demonstrates equivalent lifetime to spin coated devices of a similar architecture[24, 31].

4. Conclusions

In this work, we demonstrated the suitability of a slot-die coating method for the deposition of lead halide perovskite layers in one step and in air. Furthermore, we reported the use of an industrial 2.6 m belt oven for the annealing of such layers. We studied the effect of the substrate temperature and a cold air knife over the deposited layer, finding that a substrate at 65°C and the application of the air knife give a major control over the crystallisation process leading to important improvement of the layer features. In particular, we ascribed such result to the creation of a temperature gradient through the coated precursor solution that drives the crystallisation resulting in a thinning and flatening effect and improving the overall surface coverage of the deposition. We found the performance of devices where the perovskite layer is fully processed in air with a slot-die to be comparable to that of cells with spin coated perovskite layers in nitrogen atmosphere. The slot-die coated ones gave average power conversion efficiency of 7% and fill factor of 65.8%, with the best performing device showing a 9.2% PCE and FF of 75.6%. For the best devices, not encapsulated, after more than 1000 hours, a PCE reduction of 25.5% was observed. Such a result is completely in agreement with the 28% PCE drop after 1000 h testing for devices with the same architecture but processed in the glove box, stored in the dark at 20% humidity, already reported in literature [30]. To our knowledge, this is one of the first works on the one-step deposition in air and through slot-die coating of mixed halide perovskite layers, on a mesoporous scaffold, reporting a study over the effect of the substrate temperature and air-knife over the process. We demonstrate that controlling properly the deposition condition is possible to cast in one step and in air, through slot-die coating, high quality perovskite layers able to give cells having performances close to those totally fabricated in under nitrogen by spin coating. Other groups have already scaled the processing of other functional layers, and we think that this work is an important step toward the scaling of the entire perovskite-based photovoltaic technology.

5. Acknowledgments

The authors would like to acknowledge the Ser Cymru national research network in Advanced Engineering Materials and the EPSRC Supergen Flexible funding (EP/J017361/1). We would also like to acknowledge the assistance provided by the Swansea University AIM Facility, which was funded in part by the EPSRC (EP/M028267/1), the European Regional Development Fund through the Welsh Government (80708) and the Ser Solar project via Welsh Government.

6. References

[1] N. Espinosa, M. Hösel, D. Angmo, F. C. Krebs, Solar cells with one-day energy payback for the factories of the future, Energy Environ. Sci. 5 (1) (2012) 5117–5132. doi:10.1039/C1EE02728J.

[2] C. J. Emmott, A. Urbina, J. Nelson, Environmental and economic assessment of ITO-free electrodes for organic solar cells, Solar Energy Materials and Solar Cells 97 (2012) 14–21. doi:10.1016/j.solmat.2011.09.024.

[3] N. Espinosa, L. Serrano-Luján, A. Urbina, F. C. Krebs, Solution and vapour deposited lead perovskite solar cells: Ecotoxicity from a life cycle assessment perspective, Solar Energy Materials and Solar Cells 137 (2015) 303–310. doi:10.1016/j.solmat.2015.02.013.

[4] M. M. Lee, J. Teuscher, T. Miyasaka, T. N. Murakami, H. J. Snaith, Efficient hybrid solar cells based on meso-superstructured organometal halide perovskites., Science (New York, N.Y.) 338 (6107) (2012) 643–7. doi:10.1126/science.1228604.

[5] H.-S. Kim, C.-R. Lee, J.-H. Im, K.-B. Lee, T. Moehl, A. Marchioro, S.-J. Moon, R. Humphry-Baker, J.-H. Yum, J. E. Moser, M. Grätzel, N.-G. Park, Lead Iodide Perovskite Sensitized All-Solid-State Submicron Thin Film Mesoscopic Solar Cell with Efficiency Exceeding 9%, Scientific 2 (2012) 1–7. doi:10.1038/srep00591.

[6] W. S. Yang, J. H. Noh, N. J. Jeon, Y. C. Kim, S. Ryu, J. Seo, S. I. Seok, High-performance photovoltaic perovskite layers fabricated through intramolecular exchange, Science (May) (2015) science.aaa9272–. doi:10.1126/science.aaa9272.

[7] K. Cao, Z. Zuo, J. Cui, Y. Shen, T. Moehl, S. M. Zakeeruddin, M. Grätzel, M. Wang, Efficient Screen Printed Perovskite Solar Cells Based on Mesoscopic TiO2/Al2O3/NiO/carbon Architecture, Nano Energydoi:10.1016/j.nanoen.2015.08.009.

[8] T. Leijtens, G. E. Eperon, S. Pathak, A. Abate, M. M. Lee, H. J. Snaith, Overcoming ultraviolet light instability of sensitized TiO with meso-superstructured organometal tri-halide perovskite solar cells., Nature communications 4 (2013) 2885. doi:10.1038/ncomms3885.

[9] A. Mei, X. Li, L. Liu, Z. Ku, T. Liu, Y. Rong, M. Xu, M. Hu, J. Chen, Y. Yang, M. Grätzel, H. Han, A hole-conductor-free, fully printable mesoscopic perovskite solar cell with high stability., Science (New York, N.Y.) 345 (6194) (2014) 295–8. doi:10.1126/science.1254763.

[10] S. N. Habisreutinger, T. Leijtens, G. E. Eperon, S. D. Stranks, R. J. Nicholas, H. J. Snaith, Carbon nanotube/polymer composite as a highly stable charge collection layer in perovskite solar cells., Nano letters 14 (10) (2014) 5561–5568. doi:10.1021/nl501982b.

[11] J. Troughton, D. Bryant, K. Wojciechowski, M. J. Carnie, H. Snaith, D. A. Worsley, T. M. Watson, Highly efficient, flexible, indium-free perovskite solar cells employing metallic substrates, J. Mater. Chem. A 3 (17) (2015) 9141–9145. doi:10.1039/C5TA01755F.

[12] T. M. Schmidt, T. T. Larsen-Olsen, J. E. Carlé, D. Angmo, F. C. Krebs, Upscaling of Perovskite Solar Cells: Fully Ambient Roll Processing of Flexible Perovskite Solar Cells with Printed Back Electrodes, Advanced Energy Materials 5 (15) (2015) n/a–n/a. doi:10.1002/aenm.201500569.

[13] F. C. Krebs, Fabrication and processing of polymer solar cells: A review of printing and coating techniques, Solar Energy Materials and Solar Cells 93 (4) (2009) 394–412. doi:10.1016/j.solmat.2008.10.004.

[14] J. Baker, D. Deganello, D. T. Gethin, T. M. Watson, Flexographic printing of graphene nanoplatelet ink to replace platinum as counter electrode catalyst in flexible dye sensitised solar cell, Materials Research Innovations 18 (2) (2014) 86–90. doi:10.1179/1433075X14Y.0000000203.

[15] S. Razza, F. Di Giacomo, F. Matteocci, L. Cinà, A. L. Palma, S. Casaluci, P. Cameron, A. D'Epifanio, S. Licoccia, A. Reale,

T. M. Brown, A. Di Carlo, Perovskite solar cells and large area modules (100cm2) based on an air flow-assisted PbI2 blade coating deposition process, Journal of Power Sources 277 (2015) 286–291. doi:10.1016/j.jpowsour.2014.12.008.

[16] K. E. A. Hooper, B. Smith, P. Greenwood, J. Baker, T. M. Watson, Spray PEDOT:PSS Coated Perovskite with a Transparent Conducting Electrode for Low Cost Scalable photovoltaic Devices, Materials Research Innovations Submitted (7) (2015) 482–487. doi:10.1080/14328917.2015.1105572.

[17] Y. Mouhamad, P. Mokarian-Tabari, N. Clarke, R. A. L. Jones, M. Geoghegan, Dynamics of polymer film formation during spin coating, Journal of Applied Physics 116 (12) (2014) 123513. doi:10.1063/1.4896674.

[18] A. Barrows, A. Pearson, C. Kwak, A. Dunbar, A. Buckley, D. Lidzey, Efficient planar heterojunction mixed-halide perovskite solar cells deposited via spray-deposition, Energy & Environmental Science 00 (2014) 1–7. doi:10.1039/C4EE01546K.

[19] Y. Deng, E. Peng, Y. Shao, Z. Xiao, Q. Dong, J. Huang, Scalable fabrication of efficient organolead trihalide perovskite solar cells with doctor-bladed active layers, Energy Environ. Sci. 8 (5) (2015) 1544–1550. doi:10.1039/C4EE03907F.

[20] Y. Deng, Q. Wang, Y. Yuan, J. Huang, Vivid Colorful Hybrid Perovskite Solar Cells by Doctor-Blade Coating with Perovskite Photonic Nanostructures, Mater. Horiz.doi:10.1039/C5MH00126A.

[21] H. Back, J. Kim, G. Kim, T. Kyun Kim, H. Kang, J. Kong, S. Ho Lee, K. Lee, Interfacial modification of hole transport layers for efficient large-area perovskite solar cells achieved via blade-coating, Solar Energy Materials and Solar Cells 144 (2016) 309–315. doi:10.1016/j.solmat.2015.09.018.

[22] E. W. Jones, P. J. Holliman, A. Connell, M. L. Davies, J. Baker, R. J. Hobbs, S. Ghosh, L. Furnell, R. Anthony, C. Pleydell-Pearce, A novel dimethylformamide (DMF) free bar-cast method to deposit organolead perovskite thin films with improved stability, Chem. Commun. 52 (23) (2016) 4301–4304. doi:10.1039/C5CC09859A.

[23] J. You, L. Meng, T.-B. Song, T.-F. Guo, Y. M. Yang, W.-H. Chang, Z. Hong, H. Chen, H. Zhou, Q. Chen, Y. Liu, N. De Marco, Y. Yang, Improved air stability of perovskite solar cells via solution-processed metal oxide transport layers., Nature nanotechnology 11 (1) (2015) 75–81. doi:10.1038/nnano.2015.230.

[24] T. A. Berhe, W.-n. Su, C.-H. Chen, C.-J. Pan, J. Cheng, H.-M. Chen, M.-c. Tsai, L.-Y. Chen, A. A. Dubale, B. J. Hwang, Organometal Halide Perovskite Solar Cells: Degradation and Stability, Energy Environ. Sci.doi:10.1039/C5EE02733K.

[25] M. P. de Jong, L. J. van IJzendoorn, M. J. A. de Voigt, Stability of the interface between indium-tin-oxide and poly(3,4-ethylenedioxythiophene)/poly(styrenesulfonate) in polymer light-emitting diodes, Applied Physics Letters 77 (14) (2000) 2255. doi:10.1063/1.1315344.

[26] A. Fakharuddin, F. Di Giacomo, I. Ahmed, Q. Wali, T. M. Brown, R. Jose, Role of morphology and crystallinity of nanorod and planar electron transport layers on the performance and long term durability of perovskite solar cells, Journal of Power Sources 283 (2015) 61–67. doi:10.1016/j.jpowsour.2015.02.084.

[27] D. Liu, J. Yang, T. L. Kelly, Compact layer free perovskite solar cells with 13.5% efficiency., Journal of the American Chemical Society 136 (49) (2014) 17116–22. doi:10.1021/ja508758k.

[28] B. Suarez, V. Gonzalez-Pedro, T. S. Ripolles, R. S. Sanchez, L. Otero, I. Mora-Sero, Recombination Study of Combined Halides (Cl, Br, I) Perovskite Solar Cells., The journal of physical chemistry letters 5 (10) (2014) 1628–35. doi:10.1021/jz5006797.

[29] Y. Hou, H. Zhang, W. Chen, S. Chen, C. O. R. Quiroz, H. Azimi, A. Osvet, G. J. Matt, E. Zeira, J. Seuring, N. Kausch-Busies, W. Lövenich, C. J. Brabec, Inverted, Environmentally Stable Perovskite Solar Cell with a Novel Low-Cost and Water-Free PEDOT Hole-Extraction Layer, Advanced Energy Materials 5 (15) (2015) n/a–n/a. doi:10.1002/aenm.201500543.

[30] F. X. Xie, D. Zhang, H. Su, X. Ren, K. S. Wong, M. Grätzel, W. C. H. Choy, Vacuum-assisted thermal annealing of CH3NH3PbI3 for highly stable and efficient perovskite solar cells., ACS nano 9 (1) (2015) 639–46. doi:10.1021/nn505978r.

[31] Y. S. Kwon, J. Lim, H.-J. Yun, Y.-H. Kim, T. Park, A diketopyrrolopyrrole-containing hole transporting conjugated polymer for use in efficient stable organicinorganic hybrid solar cells based on a perovskite, Energy & Environmental Science 7 (4) (2014) 1454. doi:10.1039/c3ee44174a.

[32] J. Burschka, N. Pellet, S.-J. Moon, R. Humphry-Baker, P. Gao, M. K. Nazeeruddin, M. Grätzel, Sequential deposition as a route to high-performance perovskite-sensitized solar cells., Nature 499 (7458) (2013) 316–9. doi:10.1038/nature12340.

[33] K. Hwang, Y.-S. Jung, Y.-J. Heo, F. H. Scholes, S. E. Watkins, J. Subbiah, D. J. Jones, D.-Y. Kim, D. Vak, Toward large scale roll-to-roll production of fully printed perovskite solar cells., Advanced materials (Deerfield Beach, Fla.) 27 (7) (2015) 1241–7. doi:10.1002/adma.201404598.

[34] P. R. F. Barnes, K. Miettunen, X. Li, A. Y. Anderson, T. Bessho, M. Gratzel, B. C. O'Regan, Interpretation of Optoelectronic Transient and Charge Extraction Measurements in Dye-Sensitized Solar Cells, Advanced Materials 25 (13) (2013) 1881–1922. doi:10.1002/adma.201201372.

[35] D. Turnbull, J. C. Fisher, Rate of Nucleation in Condensed Systems, The Journal of Chemical Physics 17 (1) (1949) 71–73. doi:doi:10.1063/1.1747055.

[36] M. J. Carnie, C. Charbonnaeu, M. L. Davies, B. C. O'Regan, D. A. Worsley, T. M. Watson, Performance enhancement of solution processed perovskite solar cells incorporating functionalized silica nanoparticles, Journal of Materials Chemistry A 2 (2014) 17077–17084. doi:10.1039/C4TA03387F.

[37] B. C. O'Regan, P. R. F. Barnes, X. Li, C. Law, E. Palomares, J. M. Marin-Beloqui, Optoelectronic Studies of Methylammonium Lead Io-

dide Perovskite Solar Cells with Mesoporous TiO 2 : Separation of Electronic and Chemical Charge Storage, Understanding Two Recombination Lifetimes, and the Evolution of Band Offsets during J V Hysteresis, Journal of the American Chemical Society 137 (15) (2015) 5087–5099. doi:10.1021/jacs.5b00761.

[38] S. D. Stranks, G. E. Eperon, G. Grancini, C. Menelaou, M. J. P. Alcocer, T. Leijtens, L. M. Herz, A. Petrozza, H. J. Snaith, Electron-hole diffusion lengths exceeding 1 micrometer in an organometal trihalide perovskite absorber., Science (New York, N.Y.) 342 (6156) (2013) 341–4. doi:10.1126/science.1243982.

[39] T. Baikie, Y. Fang, J. M. Kadro, M. Schreyer, F. Wei, S. G. Mhaisalkar, M. Graetzel, T. J. White, Synthesis and crystal chemistry of the hybrid perovskite (CH3NH3)PbI3 for solid-state sensitised solar cell applications, Journal of Materials Chemistry A 1 (18) (2013) 5628. doi:10.1039/c3ta10518k.